

WFC3 H BAND FILTER OPTIMIZATION

O. Lupie,
August 20, 2000

ABSTRACT

With performance optimization as the driver, we investigate how the WFC3 IR detector quantum efficiency wavelength cutoff impacts the performance of the instrument, and how the design of the H filter can be used to maximize sensitivity. This study demonstrates an important trade: to balance the desire for a cutoff at longer wavelengths (and hence to use a Nicmos-like H filter) with the need to minimize the effects of zodi, thermal and dark background. We use a modified version of the WFC3 Exposure Time Calculator to predict the performance of the instrument using various QE cutoffs, dark signals, and H filter designs. The intention of the study is to provide the basis for scientific discussion on the design of the H filter. We conclude that: 1) the H band filter cutoff in the red should fall within the detector sensitivity curve in the red, 2) the sky+thermal signal dominate the background at wavelengths less than 1.76 microns and the dark dominates at longer wavelengths - implying that the cutoff should be somewhere below 1.76 microns, 3) the impact of the cutoff wavelength in the regime between 1.70 and 1.73 is small suggesting that, for faint and extended targets, the cutoff anywhere in this range is acceptable.

1. Introduction

The WFC3 Infrared channel, an HgCdTe 1Kx1K Rockwell detector, is designed for diffraction limited performance in the near-IR: 0.85 microns to approximately 1.73 microns. This study investigates the important trade: the desire for a QE cutoff at the longest relevant wavelengths and the minimization of the competing effects of the rising thermal+dark background. Also, the red cutoff range addressed here significantly cuts in

to the accepted ground-based and NICMOS definitions of the H band filter [see Appendix 1 for a comparison of ground-based, NICMOS, and WFC3 H filter transmission curves]. The goals of this study are:

1. design a filter whose red-cutoff is not defined by the QE curve at the red cutoff wavelength. Anticipated evolution of the detector sensitivity with time as well as a temperature could introduce a temporal component to the red sensitivity, a condition which would preclude photometry at the advertised accuracy (better than 5%).
2. optimize the filter design such that the red cutoff falls at a wavelength where the the signal/noise ratio (S/N) is maximized. The OTA+WFC3 thermal background shows a dramatic increase starting at approximately 1.7 microns.
3. investigate the trades between signal and noise by sampling the parameter space around the anticipated detector sensitivity function.

2. WFC3 Instrument and Background Model

The WFC3 Exposure Time Calculator (Hanley et al., 2000) was modified to accept special user inputs: filter transmission curves, dark levels, and detector quantum efficiency functions. With this capability, the instrument performance can be investigated as a function of these parameters and their effect on the signal from various sources can be demonstrated. This section will describe the model inputs and assumptions.

2.1 *Detector Quantum Efficiency*

The WFC3 HgCdTe detector is passively cooled to a temperature of 150K, using Thermo-electric cooler stacks. To minimize the dark current, a technology has been developed by Rockwell and is discussed in more detail in the ISR WFC3-2000-04 *First Results from the New HgCdTe MBE detectors for WFC3-IR Channel (Roberto et al 2000)*. Based on laboratory measurements of a similar detector, the estimate of the HgCdTe quantum efficiency is given in Figure 1 along with the set of QE models used in this study. Although the shape of the QE falloff is not definitively known, a steep slope was selected, the shape based on the QE curves of the NICMOS detectors, precursors to the WFC3 detector. The range of the cutoff, which is defined as the wavelength at which the QE has dropped to 50% of its peak value, is 1.54 microns to 1.76 microns. Longer wavelengths are precluded by the overall design of the detector system.

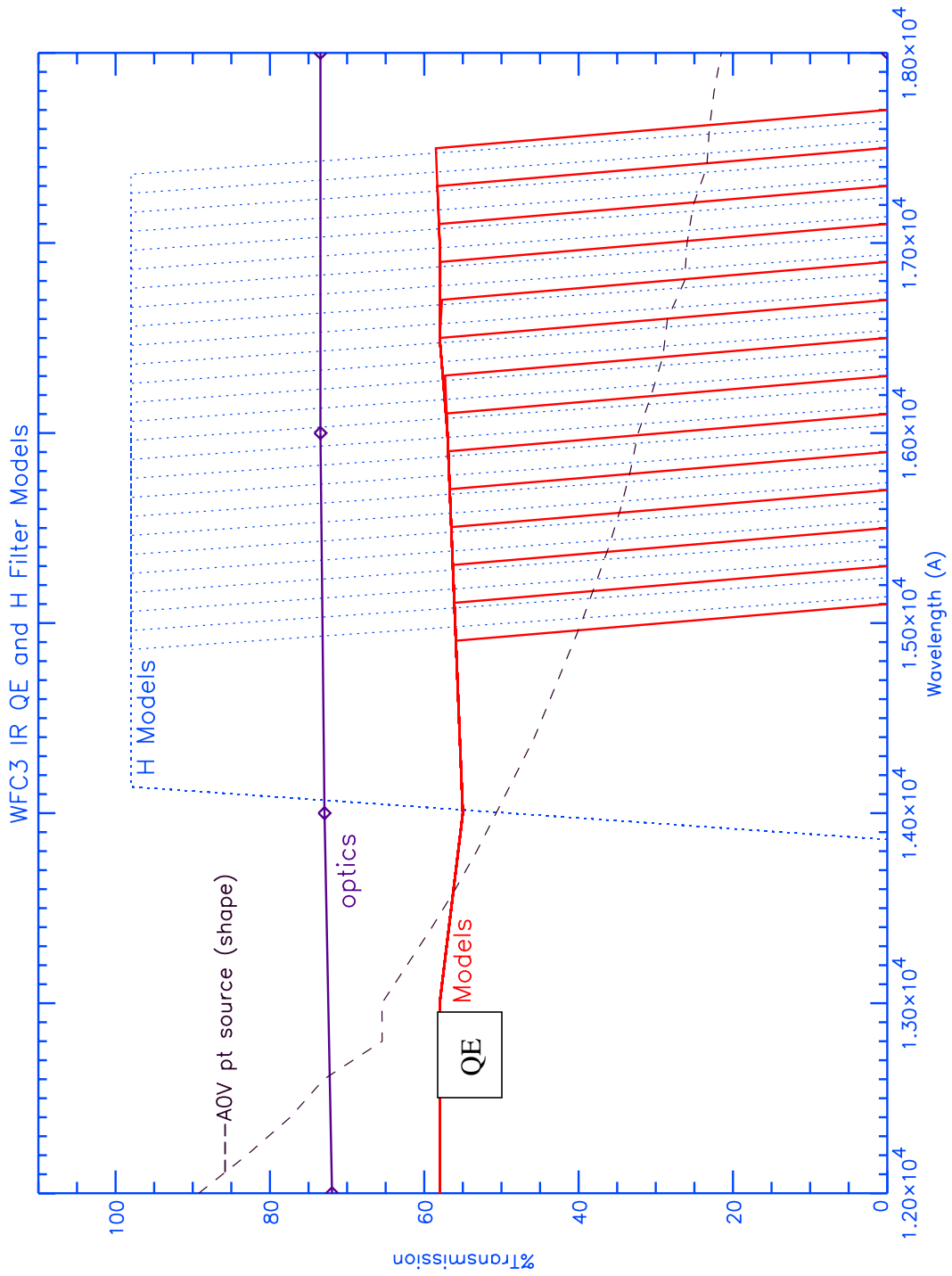


Figure 1: WFC3 QE models, H filter designs, and optics throughput as a function of wavelength (angstroms). Percent Transmission is plotted along the Y axis.

2.2 H band Filter Definition

To achieve the levels of photometry expected from the WFC3 IR channel, the H filter must lie well within the boundary of the QE curve. This requirement implies that any dependence of the QE cutoff wavelength on time or on spatial position in the detector must be taken into account when designing the H filter. The Contract End Item specifications require a QE stability of +/-1% per month [CEI 4.8.10]. Although there is little data on the QE variability of this instrument, these values are consistent with the stability as seen in other detectors of similar construction, e.g., the SIRTf detectors (Rieke, private communication).

For each detector QE model, a series of H band filters were designed with red slopes that cutoff slightly blueward of the corresponding QE cutoff wavelength. Note that all the H filter curves have the same wavelength characteristics at the blue end, i.e., the blue wavelength at the 50% peak transmission point is the same for all models, and the adjustments were made to the central wavelength and FWHM. The range of H band transmission curves are also shown in Figure 1.

2.3 Backgrounds

2.3.1 Dark Background

As mentioned in section 2.1, the HgCdTe detector dark background is directly dependent on the QE cutoff wavelength. An estimate of the functional dependence is given in Table 1 (M. Stiavelli, private communication) and shown in Figure 2. These values are appropriate for an electronic bias voltage of 250 millivolts and were derived by a semi-empirical model with parameters tuned to laboratory models (Stiavelli, private communication). We will show later how the sky+thermal background dominates the total background at wavelengths less than 1.76 microns.

Table 1. Dark Counts as a function of Detector QE cutoff (Stiavelli, private communication). The wavelength cutoff refers to the wavelength where the QE has dropped to 50% of its peak value. Note that 0.022 electrons/pix-sec was assumed to be the lowest value.

Model #	λ cutoff	electrons/pix-sec
0	1.76	0.6220
1	1.74	0.4208
2	1.72	0.3024
3	1.70	0.1840
4	1.68	0.1368
5	1.66	0.0896
6	1.64	0.0572
7	1.62	0.0396
8	1.60	0.022
9	1.58	0.022
10	1.56	0.022

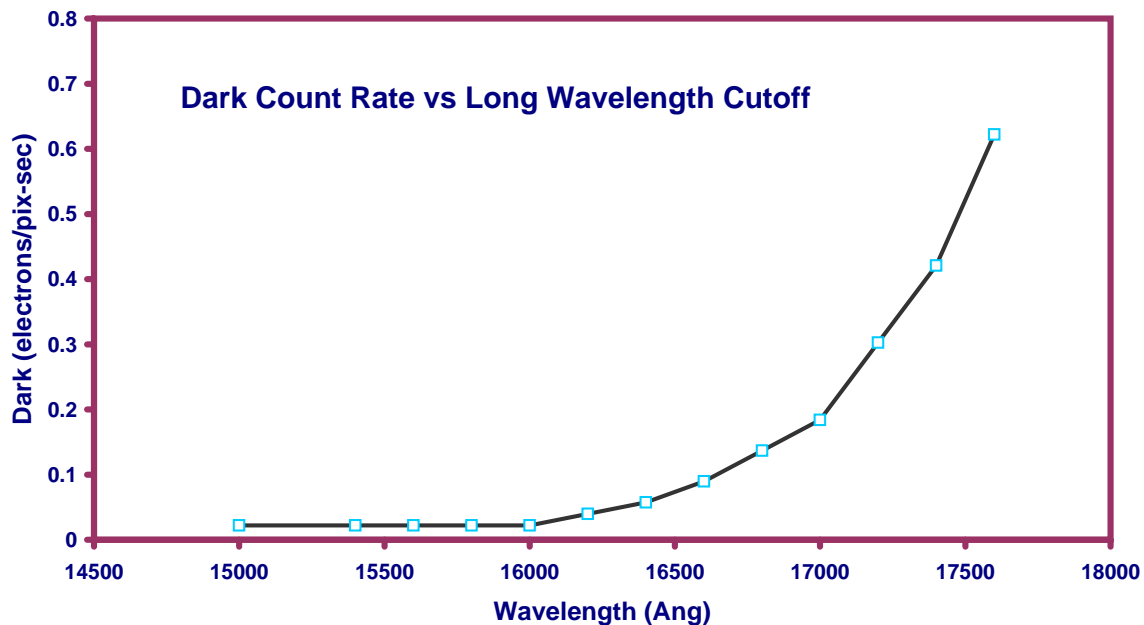


Figure 2: Estimated Dark Counts (electrons/pix-sec) as a function of Red Cutoff Wavelength.

2.3.2 OTA + WFC3 Thermal Background

A recent and robust investigation of OTA thermal emission demonstrates a close agreement between onboard flight data and the revised OTA thermal models (Robberto et al 2000). This study provides us with 1) a model of the OTA thermal emission as seen in an instrument such as WFC3, and 2) an estimate of the temporal variability of that emission as the telescope moves in its orbit and as the telescope ages (and accumulates thermally-emitting particulates and/or scatterers).

The OTA thermal model was enhanced to incorporate thermal emission from the WFC3 by scaling and modifying NICMOS thermal emission (Robberto, private communication). The adopted model as a function of wavelength provided by Robberto (and converted to

ergs/cm²-sec-A-asec²) is shown in Figure 3. Note that this model is considered conservative in that paper. A sharp rise in the detector dark redward of ~1.65 microns (figure 2) is also accompanied by a dramatic rise in the thermal emission redward of 1.7 microns. The orbital variation of the thermal emission is on the order of +/- 5% and the secular variations ~ 8%.

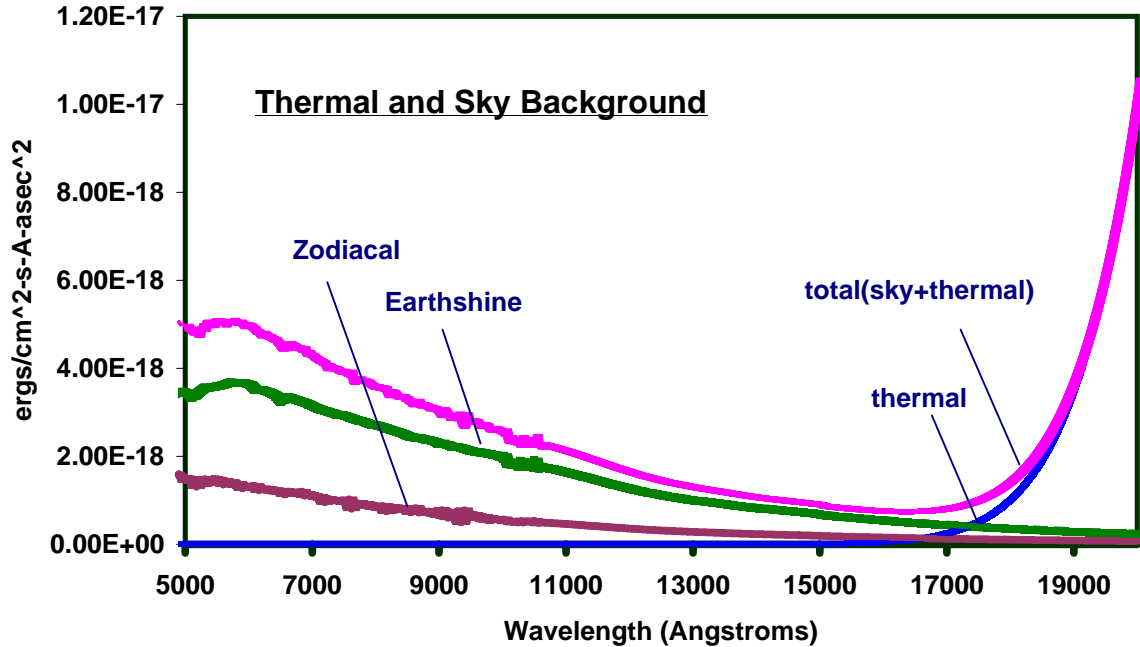


Figure 3: Comparison of OTA Thermal and Sky Backgrounds as a function of wavelength.

2.3.3 Zodiacal and EarthShine

One of the reasons the near-IR is so important to many types of astronomical investigation is because the sky background is low between 1 micron and 1.7 microns. The sky background includes:

1. zodiacal light from scattering of sunlight off dust (at near-IR wavelengths); the zodiacal flux decreases as a function of wavelength across the interval 1 to 2 microns, and
2. earthshine which decreases from 1 to 1.8 microns.

The sky background varies with the position of the earth in its orbit around the sun and with location of the target in the sky. We have used the average value of the zodiacal and

earthshine background. The average values of the Zodi and Earthshine, are shown in Figure 3 in comparison to the thermal and total (external) background contribution.

2.4 WFC3 OTA and Optical Transmission

The WFC3 IR Channel optical path contains the OTA focal plane pick-off mirror, a channel select mechanism, a pair of mirrors M1 and M2 which correct for the spherical aberration, and a refractive corrector plate. All the mirrors (with the exception of the external pick-off mirror) are coated with silver to enhance the reflectivity in the near-IR. Individual throughput estimates for these optical elements were provided by Ball Aerospace (Turner-Valle, private communication) and the combined throughput is included in the Exposure Time Calculator. The OTA throughput, verified earlier in the mission is the value provided in the STSDAS Synphot package. The combined transmission of the WFC3 optical components is included in Figure 1.

2.5 Additional Instrument Input Parameters

The Detector Read Noise is assumed to be 15 electrons per read, the gain 2 electrons/ADU. The average PSF is considered to be 5 pixels in diameter and 25 pixels in area. The detector dark values are given for 250 millivolt bias.

3. Analysis

3.1 Procedure

For each QE model, the ETC was run using the appropriate detector dark signal for that red cutoff wavelength, and a set of H-band filters. Table 2 is an example of the input data and results. for a point source, H=22, spectral type unreddened A0V. The Table 2 columns are defined as follows: Column 1 is the QE model reference number, column 2 the cutoff wavelength of the QE curve, column 3 the H filter id number, columns 4, 5, and 6 list the H filter central wavelength, FWHM, and the throughput integrated over wavelength.; columns 7 - 9, are the total number of electrons as calculated by the ETC for the source, sky, and dark respectively over the exposure time listed in column 11.; column 10 is the signal/noise (taking into account all background sources). We refer the reader back to Figure 1 for a review of the model setup.

3.2 S/N as a Function of Cutoff Wavelength

Figure 4 is a plot of the data in Table 2. The curves represent the source, dark, thermal, and sky counts as a function of detector QE cutoff wavelength during a 180 sec exposure on an A0V point source of magnitude H=22. The crossover cutoff wavelength where the dark background begins to exceed the sky background is ~ 1.76 microns. [Note, improvements in the estimation of the thermal and dark backgrounds will be monitored and this curve updated]. The exercise was repeated for a point source of magnitudes H=20, 22, and 24 and spectral type A0V, and

an extended source, H=23, 25, 25.5 magnitudes/arcsec² and spectral type 05. The extended target input assumptions were derived from the exponential profile of a disk galaxy where we integrated over an inner annulus to arrive at a signal/noise ratio.

The results for the point and extended sources are given in Figure 5 which is a plot of the S/N ratio as a function of the detector cutoff wavelength. The exposures were chosen to produce a S/N of ~10 (or 8 for the extended sources) at the longest cutoff wavelength (and hence the largest H filter design). Because of the difference in the relative contribution of the background, the functional forms of the curves are different. Based on this limited sample of objects, a cutoff wavelength could be placed anywhere in the 1.68 to 1.74 range with any significant gain or loss in S/N. However, a diagnostic which is independent of type of object would be preferred.

#	e/pix-sec		#	H	H	Area	electrons	electrons	electrons	S/N	sec
	IR QE Cutoff	Dark Current		Lambda	FWHM		source	sky	dark		Exp Time
0	17600	0.622	3	15750	3500	343000	1100	2591	2788	10.0	179.3
1	17400	0.4208	5	15650	3300	323400	1051	2399	1886	10.0	179.3
2	17200	0.3024	7	15550	3100	303800	1000	2227	1356	9.9	179.3
3	17000	0.184	9	15450	2900	284200	946	2070	825	9.7	179.3
4	16800	0.1368	11	15350	2700	264600	892	1922	614	9.4	179.3
5	16600	0.0896	13	15250	2500	245000	836	1782	402	9.0	179.3
6	16400	0.0572	15	15150	2300	225400	778	1644	256	8.5	179.3
7	16200	0.0396	17	15050	2100	205800	720	1510	178	8.0	179.3
8	16000	0.022	19	14950	1900	186200	671	1399	99	7.6	179.3
9	15800	0.022	21	14850	1700	166600	621	1288	99	7.1	179.3
10	15600	0.022	23	14750	1500	147000	537	1107	99	6.3	179.3
11	15400	0.022	25	14650	1300	127400	472	969	99	5.6	179.3
13	15000	0.022	29	14450	900	88200	335	684	99	4.1	179.3

Table 2. Source, Sky, Dark Counts, and S/N for anAOV star, H=22 as a function of QE cutoff wavelength.

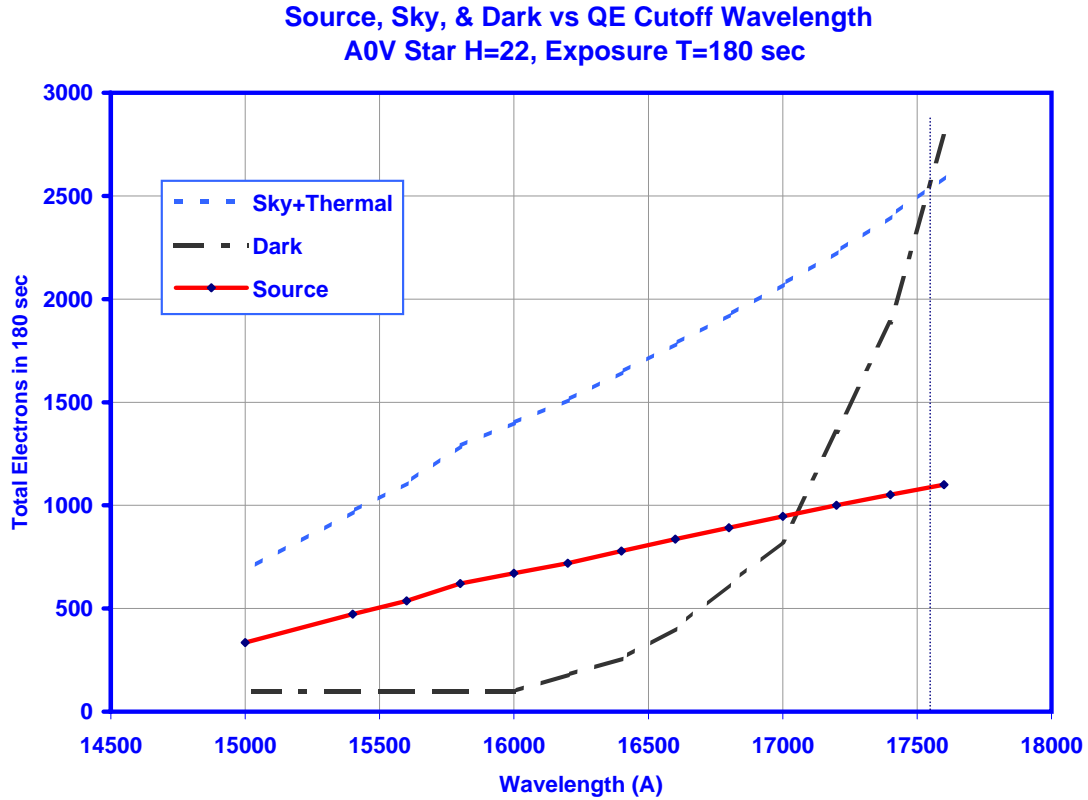


Figure 4: Source, Sky, and Dark Counts for an A0V H=22 star in 180 sec

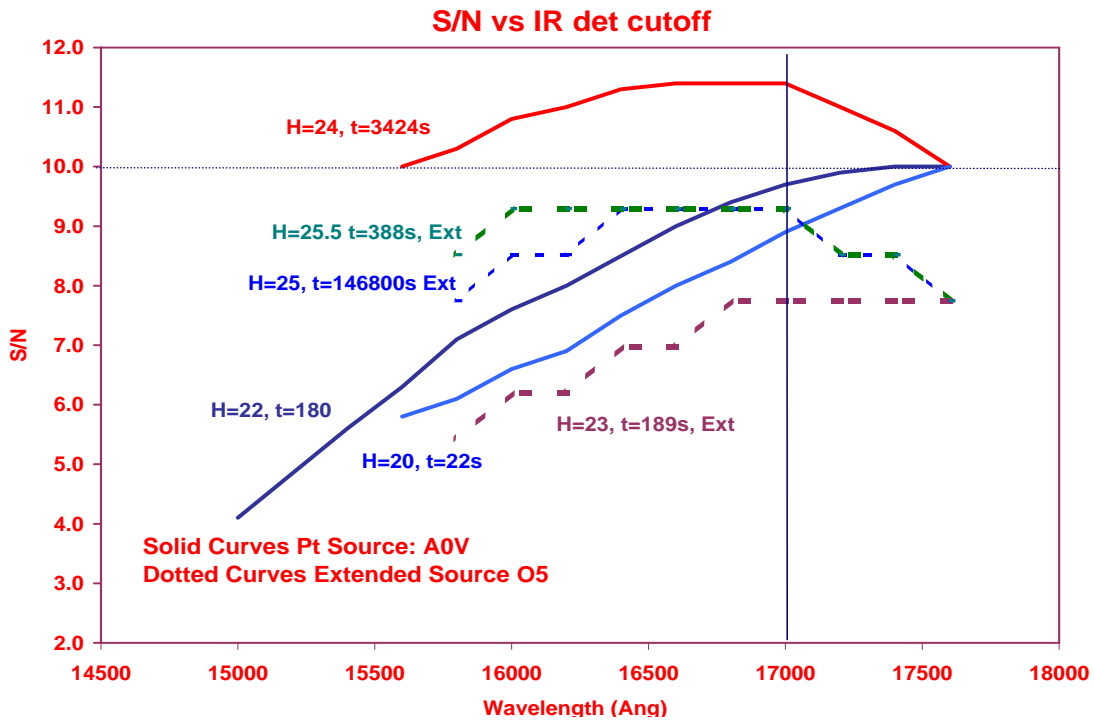


Figure 5: S/N versus QE Cutoff Wavelength for various objects and exposure times.

3.3 A Note on QE Stability and Photometry versus Cutoff Wavelength

One could speculate that the optimum cutoff wavelength is that at which any QE instability would affect the photometry the least. The CEI Specifications require that the QE stability not exceed +/- 1% over a month's time. Since we lack information about the way in which it varies, any conclusions derived using this diagnostic would be speculation only. Attributing the variability to overall quantum efficiency reduction affects the measured count rate the same way no matter what the cutoff. If we attribute the QE changes solely to the cutoff wavelength (which appears to be highly unlikely anyway, Stiavelli private communication), and keep the H filter width constant (i.e., H filter FWHM exceeds the cutoff), the change in target signal as the cutoff wavelength is varied depends on the shape of the target flux as a function of wavelength (as long as the QE+optics transmission is flat).

3.4 Comparison of J and H as a Function of Detector Cutoff

In Figure 6, we compare the S/N ratio of a point source in the J and H bands as a function of detector cutoff. Note of course that the H filter width is decreased so that it falls slightly blueward of each detector cutoff value. Also, the dark contribution is varied according to the previously discussed functional dependence on cutoff.

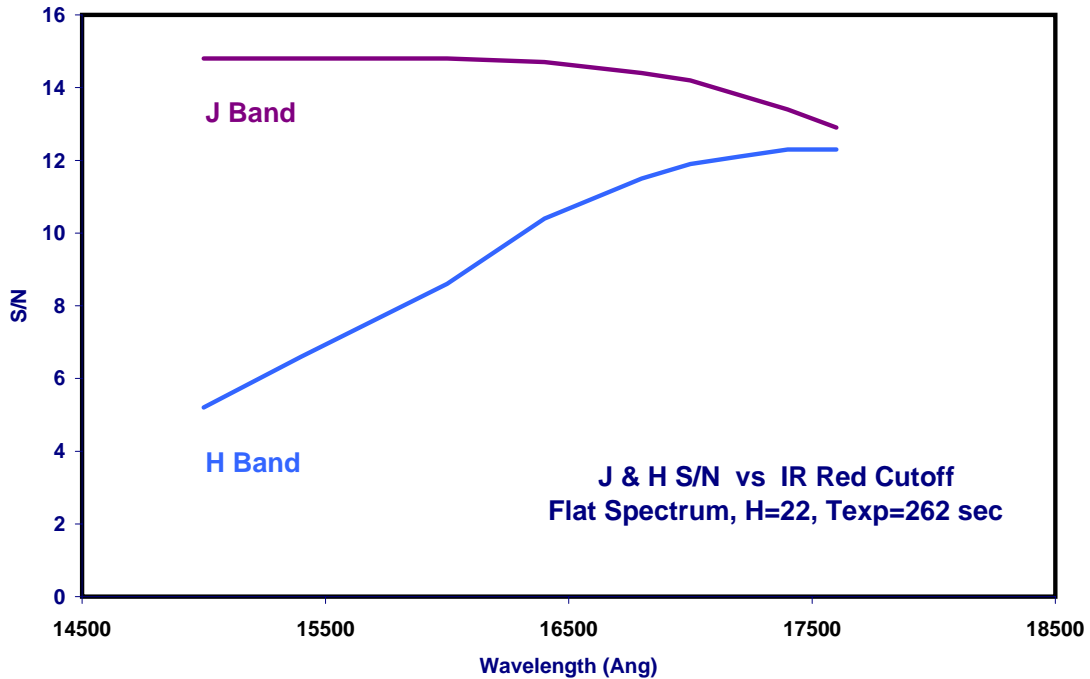


Figure 6: J and H S/N variation as the cutoff (and hence the H filter width) is varied.

The WFC3 J Band characteristics are close to the ground-based definitions:

FWHM=3000A, $\lambda_c = 1.25\mu$. On the question of transforming from one system to another, we note the following:

originally the H band filter was defined for ease of transformation to the H band filter of NICMOS rather than to ground based H filters.

ground-based H filters have a variety of widths and shapes as can be seen in the figures in the Appendix “Comparison of WFC3 H to NICMOS and Ground-Based H Bands”.

the decision was made to modify the original “NICMOS H filter” simply by adjustment of the width of the filter. We have not yet investigated quantitatively the transformation feasibility however as long as the filter transmission is well calibrated on the ground and appropriate photometric calibrations are performed in orbit, we see no complications based on the H filter specification.

4.0 Conclusions/Recommendations

We conclude the following:

- the H band filter should not define the detector sensitivity fall off in the red,
- the sky+thermal signal dominate the background at wavelengths less than 1.76 microns and the dark dominates at longer wavelengths - implying that the cutoff should be somewhere below 1.76 microns,

- the impact of the cutoff wavelength in the regime between 1.70 and 1.73 is small suggesting that, for faint and extended targets, the cutoff anywhere in this range is acceptable.
- we recommend adopting an H filter whose red-side 50% wavelength is blueward of the assumed detector cutoff by 80-160 Å to accommodate any variability of the detector QE across the detector.
- because of the uncertainties in the thermal background and QE characteristics, we also recommend consideration of the purchase of an *additional* H filter whose specifications are tailored to the actual results from ground-based testing and improved thermal modelling.

Future enhancements to these models will include a better assessment of the model accuracies, adjustments to the thermal model (anticipated to be < 10%) and experimentation using extreme values of the zodi and earthshine.

Acknowledgements: I thank M. Stiavelli for valuable reviews of this ISR and many discussions on model assumptions, and to John Mackenty, M. Roberto, and M. Giavalisco for many useful suggestions.

APPENDIX:

Comparison of WFC3 H to NICMOS and Ground-Based H Bands

Research into the H band filter has shown that its wavelength coverage is not so standard after all but it is not difficult to understand why this is the case. Ground-based filter designers have sculpted the H filter to “fit” within the confines of the near-IR atmospheric absorption (Figure A1a and Figure A1b).

There are several papers in the literature discussing the optimization of IR broad Band filters. Initially, the WFC3 H Band filter was specified by the WFC3 Scientific Oversight Committee to be very similar to the NICMOS H Filter - to minimize the transformation complexity, and in some cases to have the convenience of comparing with previously-obtained NIC exposures. The WFC3 H Band filter with red-side 50% wavelength of ~1.71 is shown in the figure for comparison.

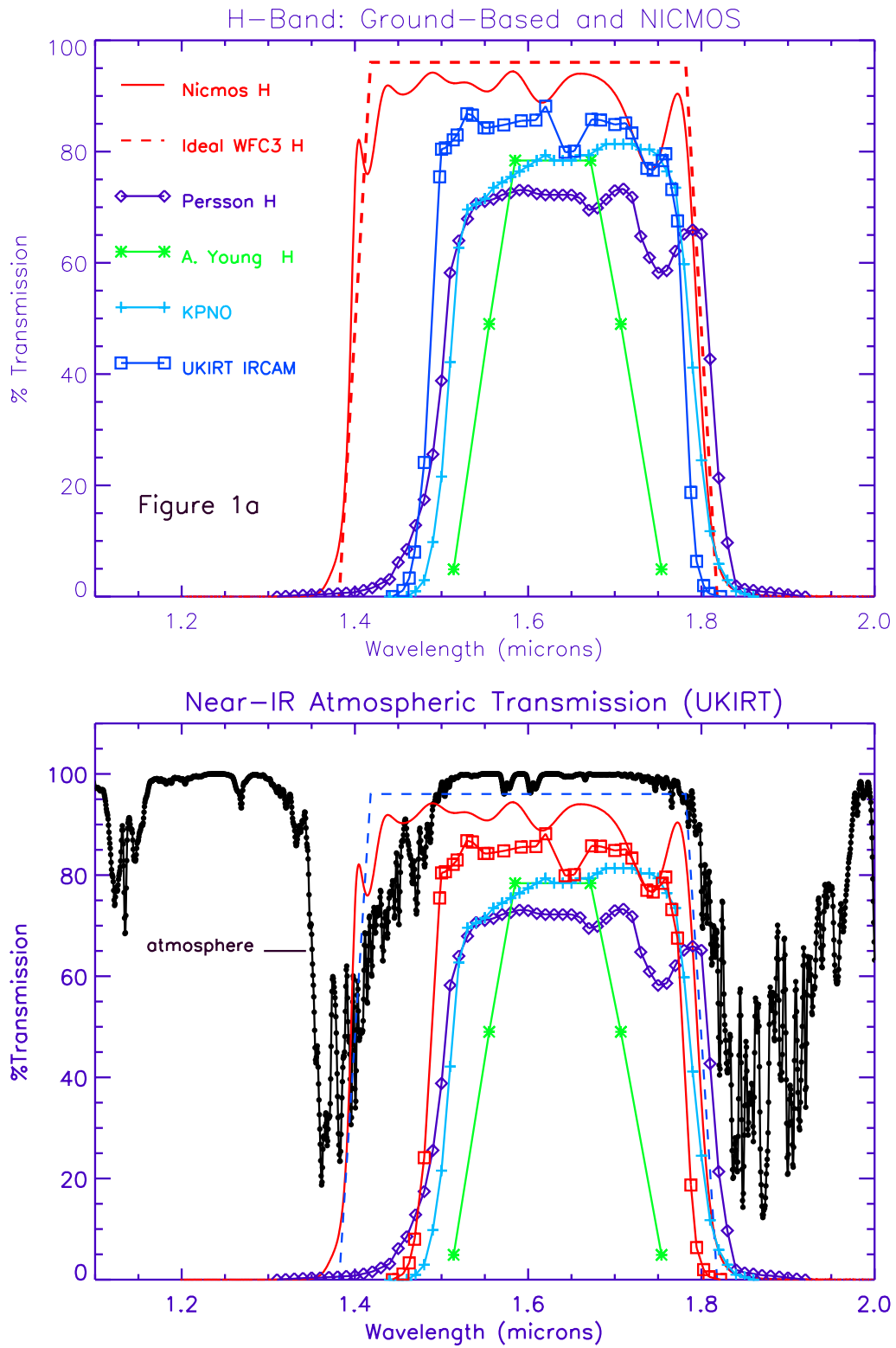


Figure A1: Ground and Space Based H filters in panel A1a and the atmospheric absorption in panel A1b.

